International Journal of
Automotive Manufacturing and Materials（IJAMM）

Scilight

Article

Parallel Cable Mechanism Adjustment Strategy between Subsystems of Space Solar Power Station

Xiangfei Ji [1,*], Guanheng Fan [2,3], Ruquan Liang [1], Jianhui Shi [1], Dengbo Zhang [1], and Yiqun Zhang [2,3]

[1] School of Mechanical & Vehicle Engineering, Linyi University, Linyi 276012, China
[2] Academy of Advanced Interdisciplinary Research, Xidian University, Xi'an 710071, China
[3] School of Mechano-Electronic Engineering, Xidian University, Xi'an 710071, China
* Correspondence: xiangfei_ji@126.com
Received: 7 July 2024; Revised: 28 August 2024; Accepted: 29 August 2024; Published: 5 September 2024

Abstract: Considering that the relative attitude between the subsystems of space solar power station has the characteristic of periodic continuous change, the adjustment strategy of space large-span parallel cable mechanism is studied. Taking OMEGA (Orb-shape Membrane Energy Gathering Array) type space solar power station as the research object, the motion relationship between subsystems is analyzed. The kinematic analysis of the cable mechanism is carried out, and the variation rule of cable length is obtained. With the minimum variance of cable force as the optimization objective, the smoothness of cable force variation and the lightweight of cable as the design criteria, the optimal installation position of cable and the optimal adjustment strategy of cable mechanism are optimized. Through simulation analysis, the parallel cable mechanism proposed in this paper changes smoothly, which is suitable for the adjustment strategy of the relative attitude of the space solar power station subsystem.

Keywords: space solar power station; parallel cable mechanism; adjustment strategy; minimum variance

1. Introduction

The development of electric vehicles has greatly reduced the pollution of automobile exhaust to the atmosphere. With the popularity of electric vehicles, the demand for electric energy will increase greatly. However, wind power generation, ground solar power generation, nuclear power and so on are subject to geographical, climate, security and other limitations. In contrast, space solar energy has unique advantages, and space solar power technology has great strategic potential.

SSPS (Space solar power station) is a technologically advanced space solution for solving energy problems. Since Dr. Peter Glaser proposed the idea of using space solar energy for power generation in 1968 [1], various research institutions have successively given their own innovative design schemes, such as SSPS reference scheme [2], sun tower configuration [3], tethered SSPS configuration [4], Integrated Symmetrical Concentrator (ISC) [5], SSPS-ALPHA [6], multi-rotary joint SSPS [7], etc., and much key technical research for their own innovative scheme have also been carried out.

OMEGA (Orb-shape Membrane Energy Gathering Array) scheme has the advantages of better heat dissipation characteristics, higher solar energy collection efficiency, and simpler subsystem attitude adjustment technology [8,9], which has attracted the attention of many scholars and carried out extensive and in-depth research. Therefore, this paper will take this scheme as the research object to carry out the corresponding research work. As shown in Figure 1, the system is an innovative scheme of spherical space solar power station based on the principle of line focusing, which includes a spherical concentrating structure for concentrating sunlight. The photovoltaic cell array (PV Array) rotates periodically on a circular orbit inside the spherical concentrating structure to maintain the orientation to the sun, and the transmitting antenna

is located in the center of the spherical concentrating structure to maintain the orientation to the earth. It can be seen that there must be relative motion between the subsystems, in which the mutual attitude between the concentrator structure and the transmitting antenna is adjusted by the upper and lower symmetric cable mechanism.

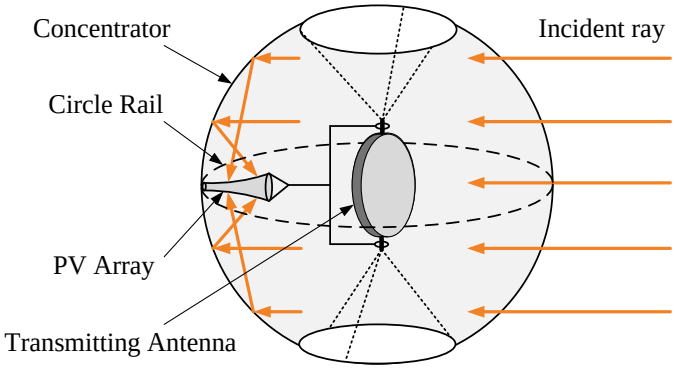

Figure 1. SSPS-OMEGA (Space Solar Power Station-Orb-shape Membrane Energy Gathering Array) scheme diagram.

Considering the structural characteristics of OMEGA scheme, the cable mechanism has two characteristics: large span and low speed continuous adjustment. In space, this kind of long-span low-speed continuous adjustment cable mechanism is very rare in the existing space systems. In the design of space deployable mechanism, flexible cable is used to maintain profile accuracy [10,11]. A similar tethered space solar power station also has a long-span connection rope, but the length of the connection rope in this system does not need to be adjusted. Even if some scholars have studied how to suppress the vibration of photovoltaic arrays by changing the connection tension, the adjustment range is very small [12,13].

In the ground system, scholars have studied deeply on the long-span rope-pulled parallel robot. S. E. Lafourcade completed the preliminary optimization design of the SACSO wind tunnel based on the accessible workspace. In the optimization process, the shape of the workspace was considered, but the impact of load on the workspace was not considered [14]. Tang et al. [15], Qiu et al. [16], and Zi et al. [17] studied the FAST (Five-hundred-meter Aperture Spherical Radio) telescope. The catenary model is used to describe the shape of the rope in the dynamic study of the rope-pulled parallel robot. At the same time, most of the redundant drives are used to achieve maximum working space, but there is no unique solution to the rope tension at this time. Mikelsons et al. [18] proposes a driving force solution algorithm, but this algorithm takes the center of gravity of convex polyhedron solution space as the optimization solution index, and deliberately gives up the search for the optimal solution. For a three-dimensional remote sensing robot (NIMS3D) that can be used for environmental monitoring, Borgstrom et al. [19] adopts the minimum 2-norm as the driving force for solving optimization objectives, but does not give specific continuity and real-time indicators. Aiming at the completely constrained positioning mechanism, Gosselin et al. [20] takes the 4-norm minimization of the deviation between each root driving force and the median driving force as the goal, and transforms the driving force distribution problem into a univariate polynomial extreme value solving problem.

To sum up, this paper carries out the design of parallel cable mechanism for OMEGA scheme. Based on the study of the interaction between the subsystems, the adjustment strategy of the cable mechanism is designed. The minimum variance of cable force is used as the optimization index to solve the cable force driven by redundant cables. The smoothness of cable force variation and cable lightweight are used as the design criteria to obtain the optimal installation position of parallel cables.

2. Coordinate System Description and Assumption

In order to facilitate the description of the mutual motion relationship between subsystems, coordinate systems are established as shown in Figure 2.

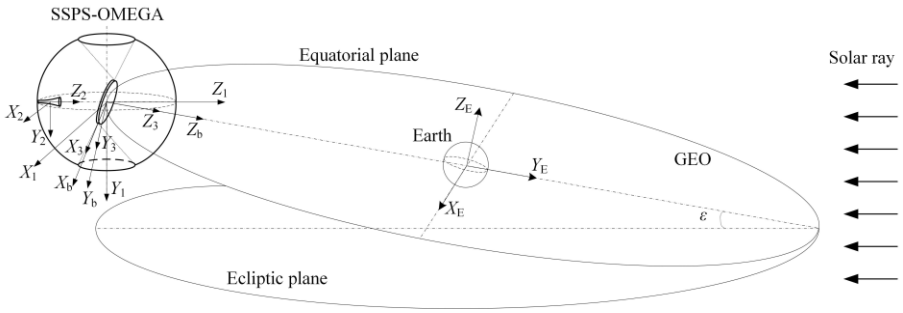

Figure 2. Coordinate systems diagram.

(1) Earth's inertial coordinate system $X_E Y_E Z_E$

The Z_E axis is perpendicular to the Earth's equatorial plane and consistent with the direction of the Earth's rotation angular velocity vector. The X_E axis is in the equatorial plane and points to the spring equinox of epoch J2000.0. The Y_E axis conforms to the right-hand rule.

(2) Concentrator coordinate system $X_1 Y_1 Z_1$ with base vextor $\boldsymbol{e}^1 = \left[\vec{e}_x^1 \quad \vec{e}_y^1 \quad \vec{e}_z^1 \right]^T$

The $X_1 Z_1$ plane coincides with the middle surface of the concentrator. The X_1 axis points to the direction in which the concentrator moves around the Earth. The Y_1 axis conforms to the right-hand rule and is coaxial with the central axis of the concentrator.

(3) PV array coordinate system $X_2 Y_2 Z_2$ with base vextor $\boldsymbol{e}^2 = \left[\vec{e}_x^2 \quad \vec{e}_y^2 \quad \vec{e}_z^2 \right]^T$

The Z_2 axis is coaxial with the rotation axis of the PV array, and points to the center of the concentrator. The Y_2 axis is in the same direction as the Y_1 axis of the concentrator coordinate system. The X_2 axis follows the right-hand rule.

(4) Transmitting antenna coordinate system $X_3 Y_3 Z_3$ with base vextor $\boldsymbol{e}^3 = \left[\vec{e}_x^3 \quad \vec{e}_y^3 \quad \vec{e}_z^3 \right]^T$

The Z_3 axis is perpendicular to the transmitting antenna plane. The X_3 axis points to the direction of the transmitting antenna relative to the Earth, is tangent to the geosynchronous (GEO) orbit, and is located in the central plane of the transmitting antenna; The Y_3 axis conforms to the right hand rule and is also located in the central plane of the transmitting antenna.

(5) Body coordinate system $X_b Y_b Z_b$ with base vextor $\boldsymbol{e}^b = \left[\vec{e}_x^b \quad \vec{e}_y^b \quad \vec{e}_z^b \right]^T$

Z_b axis is yaw axis, pointing to the center of earth. X_b axis is the rolling axis, pointing to the running direction of the SSPS-OMEGA system. Y_b axis is the pitch axis, conforming to the right-hand rule.

In the above five coordinate systems, the Earth's inertial coordinate system is the reference coordinate system; The concentrator coordinate system, the PV array coordinate system and the transmitting antenna coordinate system are the centroid coordinate systems of each subsystem of the SSPS-OMEGA system. The body coordinate system is the satellite coordinate system fixed on the SSPS-OMEGA system. In this paper, it is assumed that the transmitting antenna coordinate system and the body coordinate system completely coincide. In addition, in an ideal case, the origin of the condenser coordinate system coincides with the origin of the transmitting antenna coordinate system.

3. Planning of Relative Motion between Subsystems

As shown in Figure 3, the SSPS-OMEGA system revolves around the Earth in the GEO orbit. During the operation, the PV array needs to be oriented towards the sun, its coordinate system rotates around the Y_1 axis in the concentrator, and the Z_2 axis is always inversely parallel to the incident light, and the trajectory of the PV array in the condenser is parallel to the ecliptic plane. The transmitting antenna remains oriented to

the ground, and the Z_3 axis of the coordinate system always points to the O_E of the Earth's inertial coordinate system, so the transmitting antenna coordinate system always coincides with the system body coordinate system under ideal conditions. The origin of the concentrator coordinate system always coincides with the origin of the transmitting antenna coordinate system. However, due to the existence of the ecliptic Angle, the mutual attitude between the concentrator and the transmitting antenna will change, which is realized by changing the length of the connecting cable between them.

Figure 3 shows the position and attitude relationship between the coordinate systems of each subsystem at four-time nodes (0 h, 6 h, 12 h, 18 h) in a day. It can be seen that there is an attitude angle whose amplitude is equal to the angle of the ecliptic at each of the four-time nodes. For PV cell array, the change of the attitude angle between it and the system body coordinate system can be seen as the superposition of the attitude angle between the condenser and the system body coordinate system and the attitude angle between the PV array and the condenser, that is, the first step is to convert the system body coordinate system by rotating one certain angle to the condenser coordinate system. The second step is to convert the condenser coordinate system to the PV array coordinate system by rotating one certain angle.

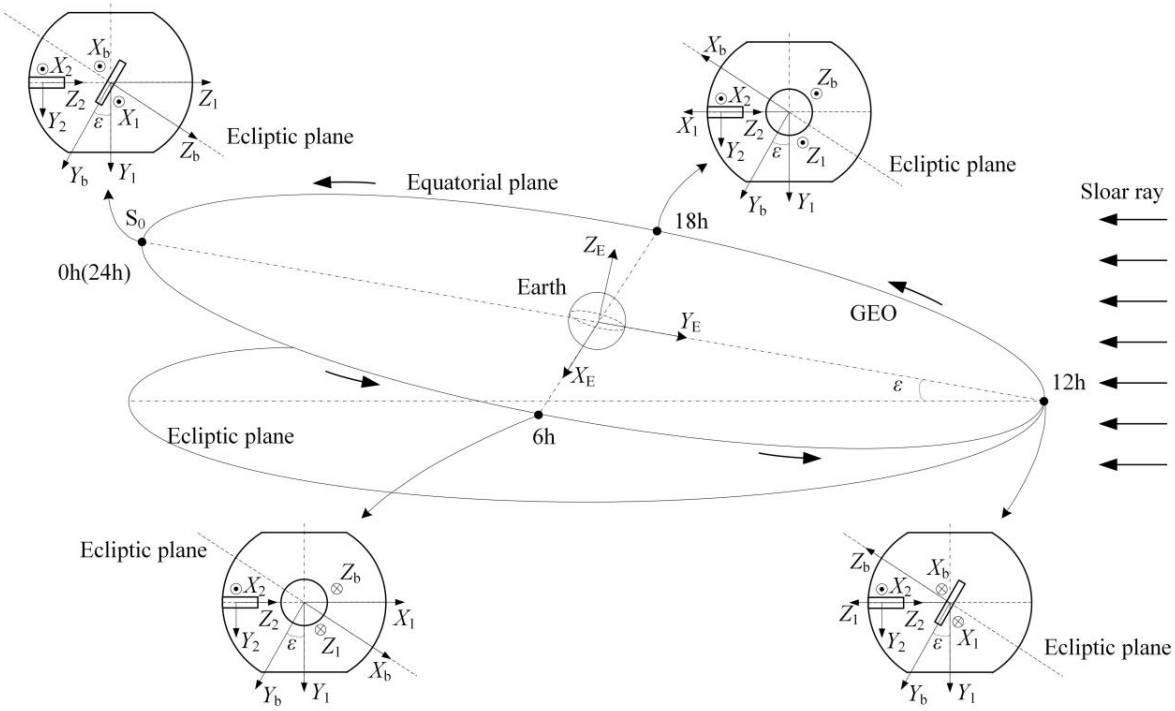

Figure 3. Diagram of relative attitude of subsystems in one day.

3.1. Attitude of the Condenser Relative to the System Body Coordinate System

As shown in Figure 4, in the heliocentric coordinate system $X_S Y_S Z_S$, the base vector of the condenser coordinate system could be expressed as:

$$\begin{cases} \vec{e}_x^{1\to S} = \begin{bmatrix} \cos\omega_E t & \sin\omega_E t & 0 \end{bmatrix}^T \\ \vec{e}_y^{1\to S} = \begin{bmatrix} 0 & 0 & -1 \end{bmatrix}^T \\ \vec{e}_z^{1\to S} = \begin{bmatrix} -\sin\omega_E t & \cos\omega_E t & 0 \end{bmatrix}^T \end{cases} \tag{1}$$

where ω_E is the angular velocity of the earth's rotation.

$\boldsymbol{A}^{(1S)}$ is the cosine matrix of the direction of the concentrator coordinate system relative to the heliocentric coordinate system, which can be obtained by Equation (2):

$$\begin{bmatrix} \vec{e}_x^1 & \vec{e}_y^1 & \vec{e}_z^1 \end{bmatrix}^T = \boldsymbol{A}^{(1S)} \begin{bmatrix} \vec{e}_x^{1\to S} & \vec{e}_y^{1\to S} & \vec{e}_z^{1\to S} \end{bmatrix}^T \tag{2}$$

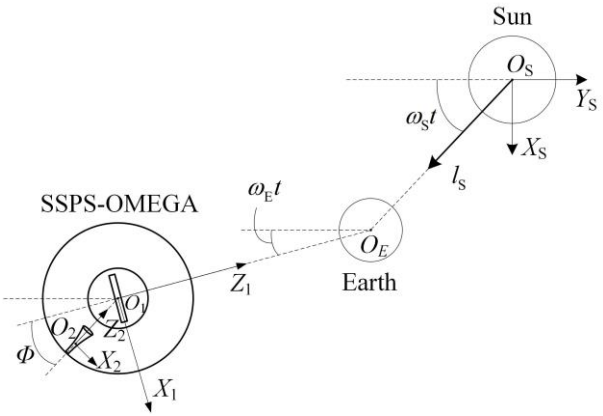

Figure 4. Diagram of mutual motion between the system, the Sun and the Earth.

At the same time, $\boldsymbol{A}^{(1S)}$ could also be expressed as:

$$\boldsymbol{A}^{(1S)} = \boldsymbol{A}^{(1b)}\boldsymbol{A}^{(bE)}\boldsymbol{A}^{(ES)} \tag{3}$$

where

$$\boldsymbol{A}^{(ES)} = \begin{bmatrix} 1 & 0 & 0 \\ 0 & \cos\varepsilon & -\sin\varepsilon \\ 0 & \sin\varepsilon & \cos\varepsilon \end{bmatrix} \tag{4}$$

$$\boldsymbol{A}^{(bE)} = \begin{bmatrix} \cos\omega_E t & 0 & \sin\omega_E t \\ -\sin\omega_E t & 0 & -1 \\ 0 & \cos\omega_E t & 0 \end{bmatrix} \tag{5}$$

where $\varepsilon = 23°26'$, is the intersection angle of the yellow.

The attitude of the condenser relative to the system body coordinate system is rotated according to the order of Euler angle "*x*-*y*-*z*", which could be further obtained:

$$\boldsymbol{A}^{(1b)} = \begin{bmatrix} a_{11} & a_{12} & a_{13} \\ a_{21} & a_{22} & a_{23} \\ a_{31} & a_{32} & a_{33} \end{bmatrix} = \begin{bmatrix} C\gamma_1 C\beta_1 & C\gamma_1 S\beta_1 S\alpha_1 + S\gamma_1 C\alpha_1 & -C\gamma_1 S\beta_1 C\alpha_1 + S\gamma_1 S\alpha_1 \\ -S\gamma_1 C\beta_1 & -S\gamma_1 S\beta_1 S\alpha_1 + C\gamma_1 C\alpha_1 & S\gamma_1 S\beta_1 C\alpha_1 + C\gamma_1 S\alpha_1 \\ S\beta_1 & -C\beta_1 S\alpha_1 & C\beta_1 C\alpha_1 \end{bmatrix} \tag{6}$$

where S represents sine function "sin" and C represents cosine function "cos".

The angular displacement of the condenser relative to the system body coordinate system can be expressed as:

$$\begin{cases} \alpha_1 = -\arctan\dfrac{a_{32}}{a_{33}} \\ \beta_1 = \arcsin a_{31} \\ \gamma_1 = -\arctan\dfrac{a_{21}}{a_{11}} \end{cases} \tag{7}$$

when a_{11} and a_{33} are equal to zero, α_1 and γ_1 are equal to $\pm\dfrac{\pi}{2}$ respectively which is need manual regulation.

3.2. Attitude of the PV Array Relative to the System Body Coordinate System

As shown in Figure 4, the direction vector $\vec{l}_S$ of solar rays in the heliocentric coordinate system XSYSZS can be expressed as:

$$\vec{l}_S^S = \begin{bmatrix} \sin\omega_S t & -\cos\omega_S t & 0 \end{bmatrix}^T \tag{8}$$

Convert it to the condenser coordinate system $X_1Y_1Z_1$, which can be expressed as:

$$\vec{l}_{\mathrm{S}}^{\mathrm{S}\to 1}=\boldsymbol{A}^{(1\mathrm{S})}\vec{l}_{\mathrm{S}}^{\mathrm{S}} \tag{9}$$

where the calculation $\boldsymbol{A}^{(1\mathrm{b})}$ obtained in Section 3.1 is substituted into Equation (3) to obtain $\boldsymbol{A}^{(1\mathrm{S})}=\left(\boldsymbol{A}^{(\mathrm{S}1)}\right)^{\mathrm{T}}$.

In addition, the base vector $\vec{e}_z^{\,2}$ of the PV array in the condenser coordinate system $X_1Y_1Z_1$ can be expressed as:

$$\vec{e}_z^{\,2\to 1}=\boldsymbol{A}^{(12)}\vec{e}_z^{\,2} \tag{10}$$

where $\boldsymbol{A}^{(12)}$ is the direction cosine matrix of the condenser coordinate system relative to the PV battery array coordinate system:

$$\boldsymbol{A}^{(12)}=\begin{bmatrix}\cos\Phi & 0 & \sin\Phi\\ 0 & 1 & 0\\ -\sin\Phi & 0 & \cos\Phi\end{bmatrix} \tag{11}$$

The Z_2 axis of the PV array is sun-oriented, that is, inversely parallel to the direction vector of the incident light, which can be expressed as:

$$\vec{e}_z^{\,2\to 1}\vec{l}_{\mathrm{S}}^{\mathrm{S}\to 1,\mathrm{T}}=-1 \tag{12}$$

According to Equation (12), during the operation of the SSPS-OMEGA system around the Earth, the rotation angle of the PV array around the condenser is as follows:

$$\Phi=\omega_{\mathrm{E}}t \tag{13}$$

For the attitude change between the PV array coordinate system and the body coordinate system, it can be obtained by the direction cosine matrix between them, namely:

$$\boldsymbol{A}^{(2\mathrm{b})}=\boldsymbol{A}^{(21)}\boldsymbol{A}^{(1\mathrm{b})} \tag{14}$$

At the same time, the attitude of the PV array relative to the system body coordinate system is rotated according to the order of "*z*-*x*-*y*" of the Euler angle, and it can be obtained:

$$\boldsymbol{A}^{(2\mathrm{b})}=\begin{bmatrix}b_{11} & b_{12} & b_{13}\\ b_{21} & b_{22} & b_{23}\\ b_{31} & b_{32} & b_{33}\end{bmatrix}=\begin{bmatrix}-\mathrm{S}\gamma_2\mathrm{S}\beta_2\mathrm{S}\alpha_2+\mathrm{C}\gamma_2\mathrm{C}\alpha_2 & \mathrm{S}\gamma_2\mathrm{S}\beta_2\mathrm{C}\alpha_2+\mathrm{C}\gamma_2\mathrm{S}\alpha_2 & -\mathrm{S}\gamma_2\mathrm{C}\beta_2\\ -\mathrm{C}\beta_2\mathrm{S}\alpha_2 & \mathrm{C}\beta_2\mathrm{C}\alpha_2 & \mathrm{S}\beta_2\\ \mathrm{C}\gamma_2\mathrm{S}\beta_2\mathrm{S}\alpha_2+\mathrm{S}\gamma_2\mathrm{C}\alpha_2 & -\mathrm{C}\gamma_2\mathrm{S}\beta_2\mathrm{C}\alpha_2+\mathrm{S}\gamma_2\mathrm{S}\alpha_2 & \mathrm{C}\gamma_2\mathrm{C}\beta_2\end{bmatrix} \tag{15}$$

The angular displacement of the PV array coordinate system in the body coordinate system can be expressed as:

$$\begin{cases}\alpha_2=-\arctan\dfrac{b_{21}}{b_{22}}\\ \beta_2=\arcsin b_{23}\\ \gamma_2=-\arctan\dfrac{b_{13}}{b_{33}}\end{cases} \tag{16}$$

when b_{22} and b_{33} are equal to zero, α_2 and γ_2 are equal to $\pm\dfrac{\pi}{2}$ respectively which is need manual regulation.

4. Analysis and Design of Parallel Cable Mechanism

Assuming that the cable is always in a tensioned state, the cable can be approximated as a straight line in the absence of gravity in space.

4.1. Kinematics Analysis of Parallel Cable Mechanism

As shown in Figure 5, the connection point coordinates of the *j*th connecting cable with the condenser and the transmitting antenna are respectively $\vec{V}_j^{\,\mathrm{b}}=\begin{bmatrix}x_j & y_j & z_j\end{bmatrix}^{\mathrm{T}}$ and $\vec{U}_j^{\,\mathrm{b}}=\begin{bmatrix}x_j & y_j & z_j\end{bmatrix}^{\mathrm{T}}, j=1,2,\cdots,m$ in the system body coordinate system.

Accordingly, the direction vector of the *j*th cable in the system body coordinate system can be written as:

$$\vec{L}_j^{\,\mathrm{b}}=\vec{U}_j^{\,\mathrm{b}}-\vec{V}_j^{\,\mathrm{b}} \tag{17}$$

Among them, the transmit antenna coordinate $X_3Y_3Z_3$ coincides with the system body coordinate $X_bY_bZ_b$, so $\vec{U}_j^b = \vec{U}_j^3$. $\vec{V}_j^b$ can be expressed as:

$$\vec{V}_j^b = \vec{r}_1^b + \boldsymbol{A}^{(b1)}\vec{V}_j^1 \tag{18}$$

where, $\vec{V}_j^1$ is the coordinate of the connection point between the *j*th cable and the condenser in the condenser coordinate system.

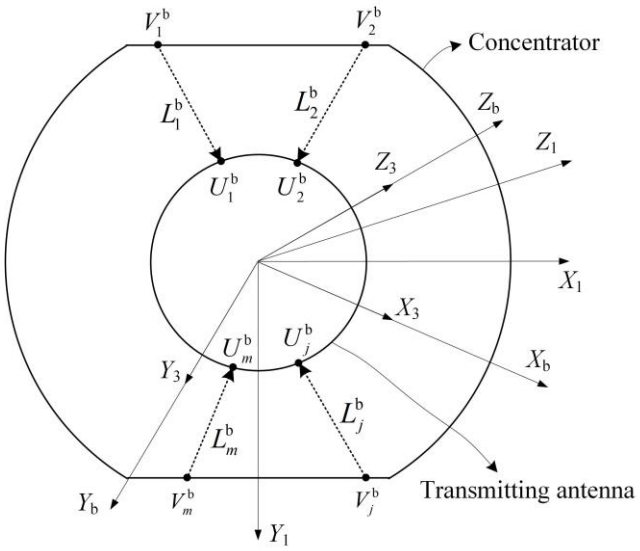

Figure 5. Diagram of the connecting cable mechanism between the condenser and the transmitting antenna.

Therefore, the length of the *j*th cable can be obtained by Equation (17). The length of the cable and the change rate can be obtained by derivation of Equation (17):

$$\dot{L}_j\vec{l}_j^b + L_j\dot{\vec{l}}_j^b = \dot{\vec{U}}_j^b - \dot{\vec{r}}_1^b - \dot{\boldsymbol{A}}^{(b1)}\vec{V}_j^1 - \boldsymbol{A}^{(b1)}\dot{\vec{V}}_j^1 \tag{19}$$

where $\dot{L}_j$ is the length change rate of the cable and $\vec{l}_j^b$ is the unit direction vector of the cable.

Taking into account $\dot{\vec{V}}_j^1 = 0$ and $\dot{\vec{U}}_j^b = 0$, Equation (19) can be rewritten as:

$$\begin{aligned} &\dot{L}_j\vec{l}_j^b + L_j\dot{\vec{l}}_j^b = -\dot{\vec{r}}_1^b - \dot{\boldsymbol{A}}^{(b1)}\vec{V}_j^1 \\ &= -\dot{\vec{r}}_1^b - \boldsymbol{A}^{(b1)}\boldsymbol{A}^{(1b)}\dot{\boldsymbol{A}}^{(b1)}\vec{V}_j^1 \\ &= -\dot{\vec{r}}_1^b - \boldsymbol{A}^{(b1)}\tilde{\vec{\omega}}_1^b\vec{V}_j^1 \\ &= -\dot{\vec{r}}_1^b + \boldsymbol{A}^{(b1)}\tilde{\vec{V}}_j^1\vec{\omega}_1^b \end{aligned} \tag{20}$$

where $\tilde{\vec{V}}_j^1$ is the component matrix of the vector $\vec{V}_j^1$.

By left multiplying both sides of Equation (20) simultaneously with $\vec{l}_j^{b,T}$, it can be get as follows:

$$\dot{L}_j\vec{l}_j^{b,T}\vec{l}_j^b + L_j\vec{l}_j^{b,T}\dot{\vec{l}}_j^b = -\vec{l}_j^{b,T}\dot{\vec{r}}_1^b + \vec{l}_j^{b,T}\boldsymbol{A}^{(b1)}\tilde{\vec{V}}_j^1\vec{\omega}_1^b \tag{21}$$

where $\vec{l}_j^{b,T}\dot{\vec{l}}_j^b = \vec{l}_j^{b,T}\left(\vec{\omega}\times\vec{l}_j^b\right) = 0$. It can be further obtained as follows:

$$\dot{L}_j = -\vec{l}_j^{b,T}\dot{\vec{r}}_1^b + \vec{l}_j^{b,T}\boldsymbol{A}^{(b1)}\tilde{\vec{V}}_j^1\vec{\omega}_1^b = \begin{bmatrix} -\vec{l}_j^{b,T} & \vec{l}_j^{b,T}\boldsymbol{A}^{(b1)}\tilde{\vec{V}}_j^1 \end{bmatrix}\begin{bmatrix} \dot{\vec{r}}_1^b \\ \vec{\omega}_1^b \end{bmatrix} \tag{22}$$

Therefore, the length change rate of all cables in the overall system can be expressed as:

$$\dot{\vec{L}} = -\boldsymbol{J}^T\dot{\vec{q}}_1^b \tag{23}$$

where $\dot{\vec{L}} = \begin{bmatrix} \dot{L}_1 & \dot{L}_2 & \cdots & \dot{L}_m \end{bmatrix}^T$, $\dot{\vec{q}}_1^b = \begin{bmatrix} \dot{\vec{r}}_1^{b,T} & \vec{\omega}_1^{b,T} \end{bmatrix}^T$,

$$\boldsymbol{J}=\begin{bmatrix} \vec{l}_1^{\,\mathrm{b}} & \vec{l}_2^{\,\mathrm{b}} & \cdots & \vec{l}_m^{\,\mathrm{b}} \\ \tilde{\vec{V}}_1^{\,1}\boldsymbol{A}^{(\mathrm{lb})}\vec{l}_1^{\,\mathrm{b}} & \tilde{\vec{V}}_2^{\,1}\boldsymbol{A}^{(\mathrm{lb})}\vec{l}_2^{\,\mathrm{b}} & \cdots & \tilde{\vec{V}}_m^{\,1}\boldsymbol{A}^{(\mathrm{lb})}\vec{l}_m^{\,\mathrm{b}} \end{bmatrix}$$

Equation (23) represents the relationship between the change rate of the generalized coordinates of the condenser relative to the system body coordinate system and the length change rate of the cable.

4.2. Redundant Cables Tension Force Solution

Without considering the influence of the subsystem flexibility factor on the mechanical characteristics of the connecting cable mechanism, the multi-body rigid body dynamics equation of the condenser and PV array system is derived [21,22] as follows:

$$\ddot{\vec{R}}_{\mathrm{b}}^{\mathrm{E}}\sum_{i=1}^{2}M_i+\sum_{i=1}^{2}M_i\ddot{\vec{r}}_i^{\,\mathrm{b}}+2\tilde{\vec{\omega}}_{\mathrm{b}}^{\mathrm{E}}\sum_{i=1}^{2}M_i\dot{\vec{r}}_i^{\,\mathrm{b}}+\dot{\tilde{\vec{\omega}}}_{\mathrm{b}}^{\mathrm{E}}\sum_{i=1}^{2}M_i\vec{r}_i^{\,\mathrm{b}}+\tilde{\vec{\omega}}_{\mathrm{b}}^{\mathrm{E}}\tilde{\vec{\omega}}_{\mathrm{b}}^{\mathrm{E}}\sum_{i=1}^{2}M_i\vec{r}_i^{\,\mathrm{b}}=\sum_{i=1}^{2}\vec{F}_{gi}+\sum_{j=1}^{m}\vec{l}_j^{\,\mathrm{b}}F_{lj} \tag{24}$$

$$\begin{aligned}&\sum_{i=1}^{2}\dot{\boldsymbol{I}}_i^{\,\mathrm{b}}\vec{\omega}_{\mathrm{b}}^{\mathrm{E}}+\sum_{i=1}^{2}\boldsymbol{I}_i^{\,\mathrm{b}}\dot{\vec{\omega}}_{\mathrm{b}}^{\mathrm{E}}+\sum_{i=1}^{2}\boldsymbol{I}_i\dot{\vec{\omega}}_i^{\,\mathrm{b}}+\sum_{i=1}^{2}M_i\tilde{\vec{r}}_i^{\,\mathrm{b}}\ddot{\vec{r}}_i^{\,\mathrm{b}}+\sum_{i=1}^{2}\tilde{\vec{\omega}}_{\mathrm{b}}^{\mathrm{E}}\boldsymbol{I}_i^{\,\mathrm{b}}\vec{\omega}_{\mathrm{b}}^{\mathrm{E}}+\sum_{i=1}^{2}\tilde{\vec{\omega}}_{\mathrm{b}}^{\mathrm{E}}\boldsymbol{I}_i^{\,\mathrm{b}}\vec{\omega}_i^{\,\mathrm{b}}+\sum_{i=1}^{2}M_i\tilde{\vec{\omega}}_{\mathrm{b}}^{\mathrm{E}}\tilde{\vec{r}}_i^{\,\mathrm{b}}\dot{\vec{r}}_i^{\,\mathrm{b}}\\&=\sum_{i=1}^{2}\vec{T}_{gi}+\sum_{j=1}^{m}\left(\vec{r}_1^{\,\mathrm{b}}+\boldsymbol{A}^{(\mathrm{b1})}\vec{V}_j^{\,1}\right)\times\vec{l}_j^{\,\mathrm{b}}F_{lj}\end{aligned} \tag{25}$$

where F_{lj} is the tension force of the jth cable.

The multi-rigid body dynamics equation of the subsystem can be further rewritten as:

$$\boldsymbol{J}_{\mathrm{b}}\vec{F}_l=\begin{bmatrix}\vec{F}\\ \vec{T}\end{bmatrix} \tag{26}$$

where $\vec{F}=\ddot{\vec{R}}_{\mathrm{b}}^{\mathrm{E}}\sum_{i=1}^{2}M_i+\sum_{i=1}^{2}M_i\ddot{\vec{r}}_i^{\,\mathrm{b}}+2\tilde{\vec{\omega}}_{\mathrm{b}}^{\mathrm{E}}\sum_{i=1}^{2}M_i\dot{\vec{r}}_i^{\,\mathrm{b}}+\dot{\tilde{\vec{\omega}}}_{\mathrm{b}}^{\mathrm{E}}\sum_{i=1}^{2}M_i\vec{r}_i^{\,\mathrm{b}}+\tilde{\vec{\omega}}_{\mathrm{b}}^{\mathrm{E}}\tilde{\vec{\omega}}_{\mathrm{b}}^{\mathrm{E}}\sum_{i=1}^{2}M_i\vec{r}_i^{\,\mathrm{b}}-\sum_{i=1}^{2}\vec{F}_{gi}$,
$\vec{T}=\sum_{i=1}^{2}\dot{\boldsymbol{I}}_i^{\,\mathrm{b}}\vec{\omega}_{\mathrm{b}}^{\mathrm{E}}+\sum_{i=1}^{2}\boldsymbol{I}_i^{\,\mathrm{b}}\dot{\vec{\omega}}_{\mathrm{b}}^{\mathrm{E}}+\sum_{i=1}^{2}\boldsymbol{I}_i\dot{\vec{\omega}}_i^{\,\mathrm{b}}+\sum_{i=1}^{2}M_i\tilde{\vec{r}}_i^{\,\mathrm{b}}\ddot{\vec{r}}_i^{\,\mathrm{b}}+\sum_{i=1}^{2}\tilde{\vec{\omega}}_{\mathrm{b}}^{\mathrm{E}}\boldsymbol{I}_i^{\,\mathrm{b}}\vec{\omega}_{\mathrm{b}}^{\mathrm{E}}+\sum_{i=1}^{2}\tilde{\vec{\omega}}_{\mathrm{b}}^{\mathrm{E}}\boldsymbol{I}_i^{\,\mathrm{b}}\vec{\omega}_i^{\,\mathrm{b}}+\sum_{i=1}^{2}M_i\tilde{\vec{\omega}}_{\mathrm{b}}^{\mathrm{E}}\tilde{\vec{r}}_i^{\,\mathrm{b}}\dot{\vec{r}}_i^{\,\mathrm{b}}-\sum_{i=1}^{2}\vec{T}_{gi}$, coefficient matrix $\boldsymbol{J}_{\mathrm{b}}=\begin{bmatrix}\vec{l}_1^{\,\mathrm{b}} & \vec{l}_2^{\,\mathrm{b}} & \cdots & \vec{l}_m^{\,\mathrm{b}}\\ \tilde{\vec{V}}_1^{\,\mathrm{b}}\vec{l}_1^{\,\mathrm{b}} & \tilde{\vec{V}}_2^{\,\mathrm{b}}\vec{l}_2^{\,\mathrm{b}} & \cdots & \tilde{\vec{V}}_m^{\,\mathrm{b}}\vec{l}_m^{\,\mathrm{b}}\end{bmatrix}$.

In the ideal case, there is no deviation between the body coordinate system and the orbital coordinate system, so when the number of cables and the number of equations are equal, the tension force of all cables can be obtained by substituting the known mutual motion position and attitude relationship between subsystems into Equation (26). When the number of cables exceeds the number of equations, there is redundant drive, and Equation (26) cannot obtain a unique solution. At this time, the tension force of the cable can be expressed as:

$$\vec{F}_l=\boldsymbol{J}_{\mathrm{b}}^{+}\begin{bmatrix}\vec{F}\\ \vec{T}\end{bmatrix}+\begin{bmatrix}\vec{\xi}_1 & \vec{\xi}_2 & \cdots & \vec{\xi}_{m-6}\end{bmatrix}\vec{c} \tag{27}$$

where $\boldsymbol{J}_{\mathrm{b}}^{+}$ is the generalized inverse matrix of $\boldsymbol{J}_{\mathrm{b}}$, $\begin{bmatrix}\vec{\xi}_1 & \vec{\xi}_2 & \cdots & \vec{\xi}_{m-6}\end{bmatrix}$ is the fundamental system of solutions of $\boldsymbol{J}_{\mathrm{b}}$, $\vec{c}=\begin{bmatrix}c_1 & c_2 & \cdots & c_{m-6}\end{bmatrix}^{\mathrm{T}}$ is the coefficient vector of the fundamental solution system.

As a component with certain elasticity, the tension force of all cables has interval constraint. In order to ensure that the cable is in a tensioning state, the tension force acting on the cable should not be less than its pretension force $F_l$min, and the material strength of the cable and the drive power of the servo motor determine the maximum tension force $F_l$max that the cable can withstand, that is, the tension force constraint on each cable is:

$$F_{l\min}\le F_{lj}\le F_{l\max} \tag{28}$$

Su et al. [23] mentioned that the minimum variance index is of the most physical significance. By adjusting the coefficient of the fundamental system of solutions, the tension force of each cable can be kept near the target value. Therefore, the optimization model can be obtained as follows:

$$\begin{aligned} \min \quad & F(\vec{c}) = \frac{1}{m}\sum_{j=1}^{m}\left(F_{lj} - F_l^*\right)^2 \\ \text{s.t.} \quad & \vec{F}_l = \boldsymbol{J}_{\mathrm{b}}^{+}\begin{bmatrix}\vec{F}\\ \vec{T}\end{bmatrix} + \begin{bmatrix}\vec{\xi}_1 & \vec{\xi}_2 & \cdots & \vec{\xi}_{m-6}\end{bmatrix}\vec{c} \\ & F_{l\min} \le F_{lj} \le F_{l\max} \quad (j = 1, 2, \cdots m) \end{aligned} \tag{29}$$

where F_l^* is the target tension force.

4.3. Cable Connection Location Design Criteria

Considering the structural symmetry and the periodicity of the relative motion between the condenser and the transmitting antenna, the connection cable mechanism scheme is designed as an eight parallel cable connection scheme. As shown in Figure 6, each side of the OMEGA has four cables connecting the condenser and the transmitting antenna. Number 1, 2, 3, 4 cables are at the up, number 5, 6, 7, 8 cables are at the down. They have the same connection point number on the condenser and the transmitting antenna. The positions of the connection points are symmetric with respect to the coordinate axis. φ is the angle between connection points at the transmitting antenna and coordinate axis. θ is the angle between connection points at the condenser and coordinate axis. Different φ and θ fitting together will form different cable mechanism adjustment methods. Here are some guidelines on how to choose the best adjustment from these combinations.

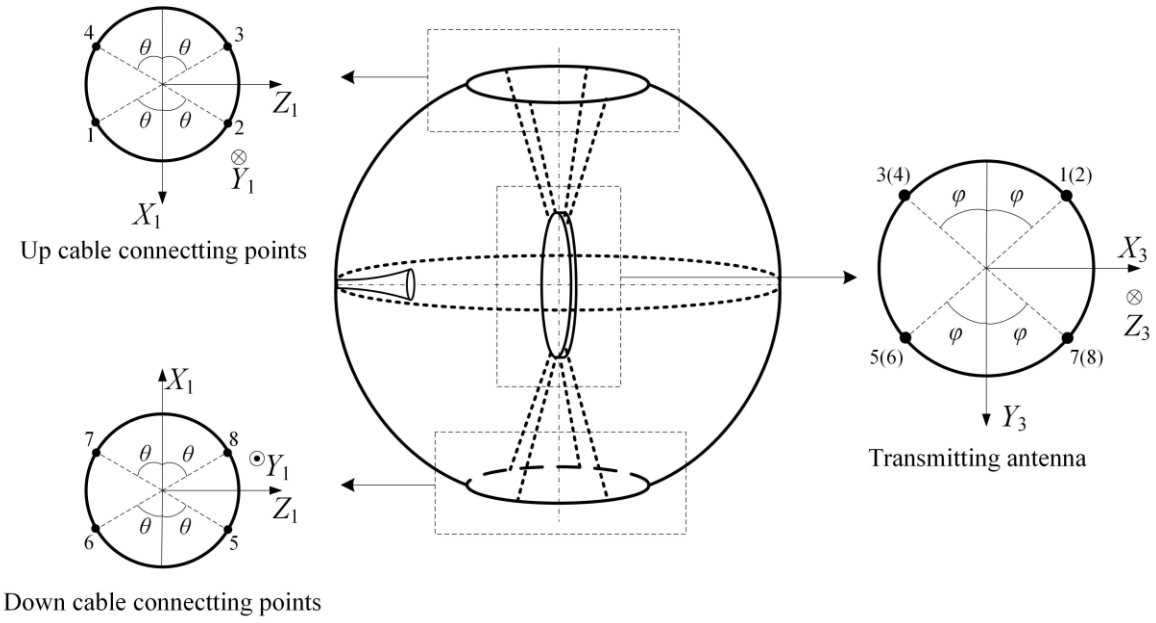

Figure 6. Diagram of eight parallel cable connection points.

(1) Cable force continuity criteria

When the relative attitude of the transmitting antenna and the condenser is adjusted continuously, if the driving force sudden changes, the relative attitude of the transmitting antenna and the condenser will cause attitude oscillation and it is very difficult to recover, which will affect the pointing accuracy of microwave beam and the solar energy collection efficiency. Within the range of one cycle change of relative attitude, the maximum tension force increment $\max\{\Delta F_{lj}\}$ of each cable with adjacent time step Δt and the maximum tension force gradient increment $\max\{\nabla F_{lj}\}$ of each cable are:

$$\max\{\Delta F_{lj}\} = \max_{0 \le t \le T}\left\| F_{lj}^{t+\Delta t} - F_{lj}^{t} \right\| \tag{30}$$

$$\max\{\nabla F_{lj}\} = \max_{\Delta t \le t \le T} \left\| \frac{F_{lj}^{t+\Delta t} - F_{lj}^{t}}{\Delta t} - \frac{F_{lj}^{t} - F_{lj}^{t-\Delta t}}{\Delta t} \right\| \tag{31}$$

If both meet:

$$\begin{cases} \max\{\Delta F_{lj}\} \le \delta_1 \\ \max\{\nabla F_{lj}\} \le \delta_2 \end{cases} \tag{32}$$

It can be considered that the tension force changes smoothly and continuously with time.

(2) Cable lightweight criteria

The rocket launch cost used in the construction of the spacecraft system is crucial, and all parts of the structure need to be lightweight as a design goal. Therefore, on the basis of satisfying the cable force smooth and continuous change, the total weight of the cable mechanism should be minimum. Considering that the reserved length of the cable must meet the maximum length in the process of cable length change, and each cable has the same density and cross-sectional area, there is

$$\min\left\{\sum_{j}^{m} L_j\right\} \tag{33}$$

5. Simulation Analysis

5.1. System Parameter

Set the power output of the ground receiving antenna as $P_0 = 2$ GW, and calculate the characteristic dimensions of each subsystem according to the predicted energy transfer efficiency link, as shown in Table 1. Since heat dissipation equipment and power transmission equipment is not designed in detail in the position of the PV array, this part of the quality is not considered in the PV. In the simulation process, the time period is set to 24 h, the time step is set to 360 s, and the upper limit of the continuity criterion is set to $\delta_1 = 2$ N, $\delta_2 = 2$ N.

Table 1. The basis parameters of 2GW SSPS-OMEGA.

Subsystems	Characteristic Dimensions (m)	Mass (kg)	Inertia (kg·m^2)
Concentrator	$R_1 = 1500$	3.53×10^6	diag([1.68×10^{13}, 1.96×10^{13}, 1.68×10^{13}])
PV array	$R_2 = 151.8$ $H_2 = 262.7$	2.01×10^6	diag([8.61×10^6, 2.73×10^4, 8.61×10^6])
Transmitting antenna	$R_3 = 500$	6.54×10^6	diag([1.88×10^7,1.88×10^7,3.77×10^7])

5.2. Subsystem Relative Attitude

Ideally, the center of mass of the condenser is assumed to coincide with the origin of the system body coordinate system. Due to the existence of the ecliptic angle, the attitude between the condenser and the system body coordinate system has a continuous periodic change, as shown in Figure 7. Among them, the change trend of attitude angle around X_b axis and Z_b axis is the same, the amplitude is equal to the declination angle (23.43°), and the period is 24 h. However, the change around X_b axis lags behind the change around Z_b axis by 6 h. The attitude angle around the Y_b axis has a amplitude of 2.36° and a period of 12 h. It can be seen that the attitude angle around the Y_b axis has a smaller change amplitude and a faster change frequency. Correspondingly, the angular velocity and angular acceleration magnitudes about the X_b axis and Z_b axis are 5.96°/h and 1.69°/h^2, respectively, and the angular velocity and angular acceleration magnitudes about the Y_b axis are 1.24°/h and 0.65°/h^2, respectively, relative to the Earth's rotation angular velocity (15°/h). The attitude angle between the condenser and the system body coordinate system (i.e., the transmitting antenna) changes slowly. At the same time, the simulation results provide a reference for the length adjustment of the connecting cables.

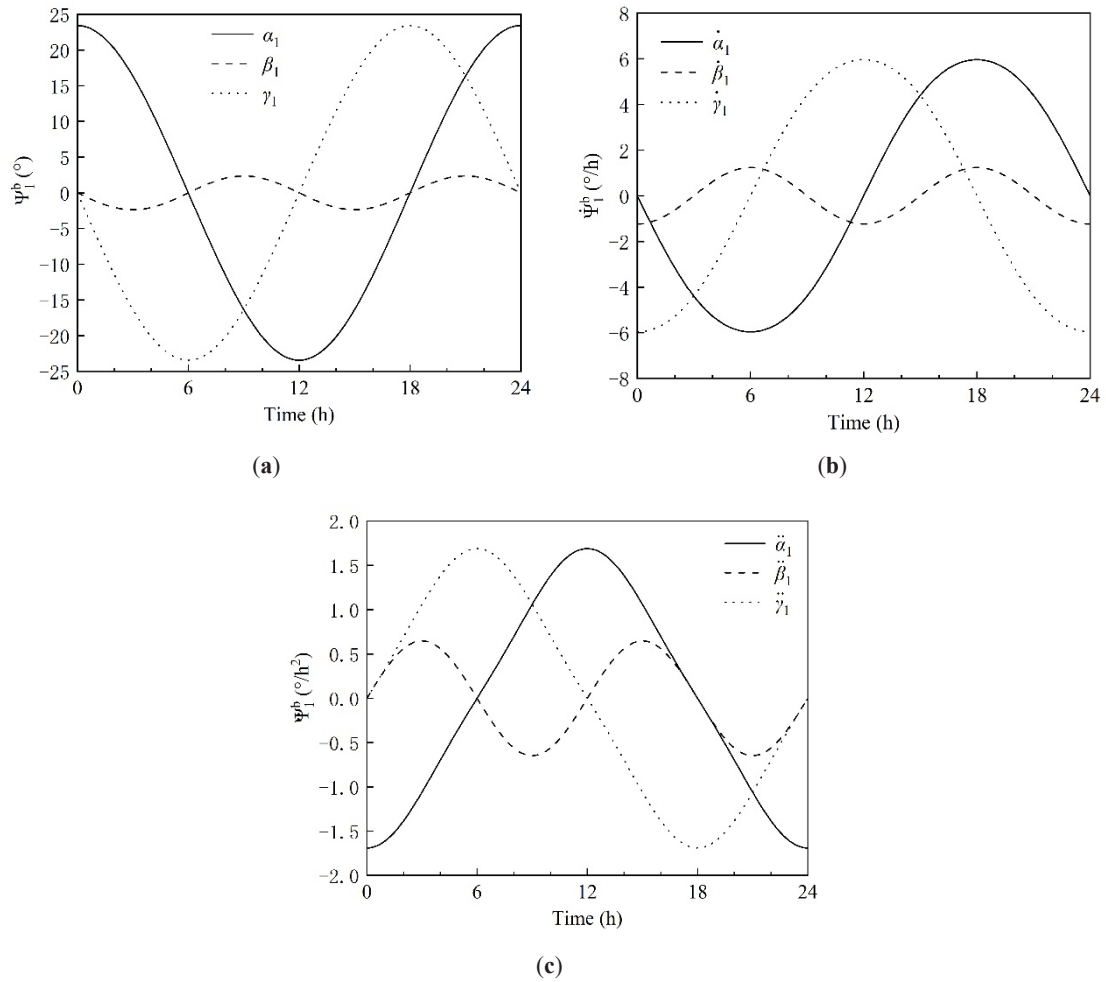

Figure 7. The angular displacement, angular velocity and angular acceleration of the condenser relative to the system body coordinate system. (**a**) Angular displacement; (**b**) Angular velocity; (**c**) Angular acceleration.

As shown in Figure 8, from the Angle of angular displacement, the change trend of attitude Angle around X_b axis and Z_b axis is similar, with a amplitude of 23.43° and a period of 24 h. However, in terms of angular velocity and angular acceleration, there is a difference between the attitude angle change around the X_b axis and the Z_b axis: the angular velocity around the X_b axis is 6.50°/h, while the angular velocity around the Z_b axis is relatively small, 5.96°/h. Moreover, around 6 and 18 h, the angular acceleration around the Z_b axis is relatively gentle, and it is also the position where the angular acceleration is the largest, with a maximum value of 1.43°/h^2, while the angular acceleration around the X_b axis is larger, with a maximum value of 1.70°/h^2. From the perspective of linear displacement, the center of mass of the photovoltaic cell array is fixed relative to the coordinates of the Y_b axis, and the coordinates in the direction of the X_b axis and the Z_b axis are periodically changed in sine and cosine form. Therefore, it can be considered that the photovoltaic cell array rotates around the Y_b axis at a non-uniform fixed axis, and the angular velocity varies periodically from 13.76 to 16.35°/h, with a period of 12 h. The angular acceleration has a amplitude of 0.68°/h^2.

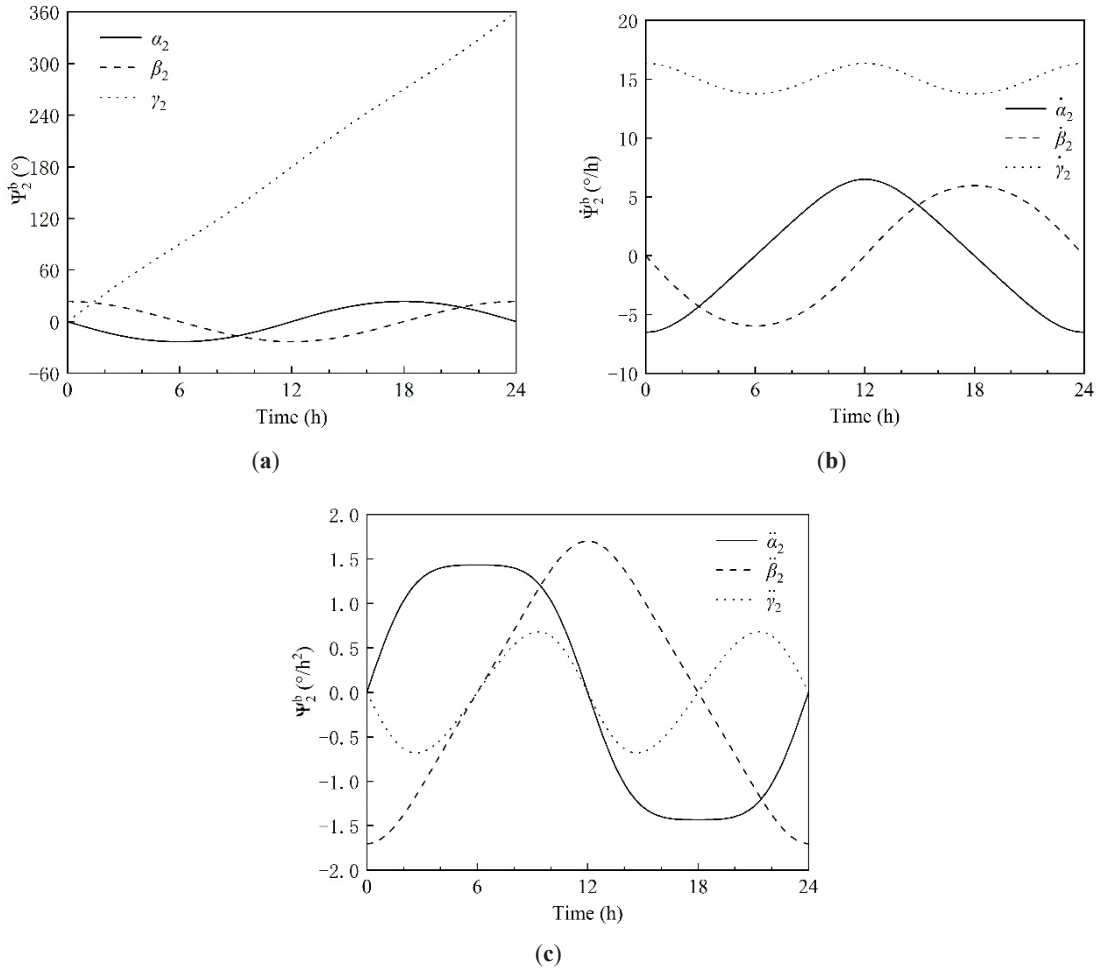

Figure 8. The angular displacement, angular velocity and angular acceleration of the PV array relative to the system body coordinate system. (**a**) Angular displacement; (**b**) Angular velocity; (**c**) Angular acceleration.

5.3. Optimal Mechanism Adjustment Strategy

By optimizing the design of the cable mechanism, the optimal eight parallel cable drive connection scheme can be obtained as $\varphi = 50°$ and $\theta = 60°$. Due to the periodicity and symmetry of the relative attitude between the condenser and the transmitting antenna, the change trend between the 1th and 5th cable, the 2th and 6th cable, the 3th and 7th cable, and the 4th and 8th cable is the same respectively, and the change period is 24 h. As shown in Figures 9 and 10, the maximum cable length is 1339 m, the maximum change amount is 289 m, and the maximum change rate of cable length is 42 m/h, which is relatively slow and stable. At the same time, 200 N is taken as the cable force optimization target in Equation (22), and the maximum cable force is set to 1000 N. Through optimization, the tension force variation law of each cable is obtained, as shown in Figure 11. It can be seen that the maximum tension force of the eight cables does not exceed 280 N, and the minimum tension is 5.4 N. The change of cable force is smooth, which is easy to adjust the relative attitude between the condenser and the transmitting antenna smoothly and continuously.

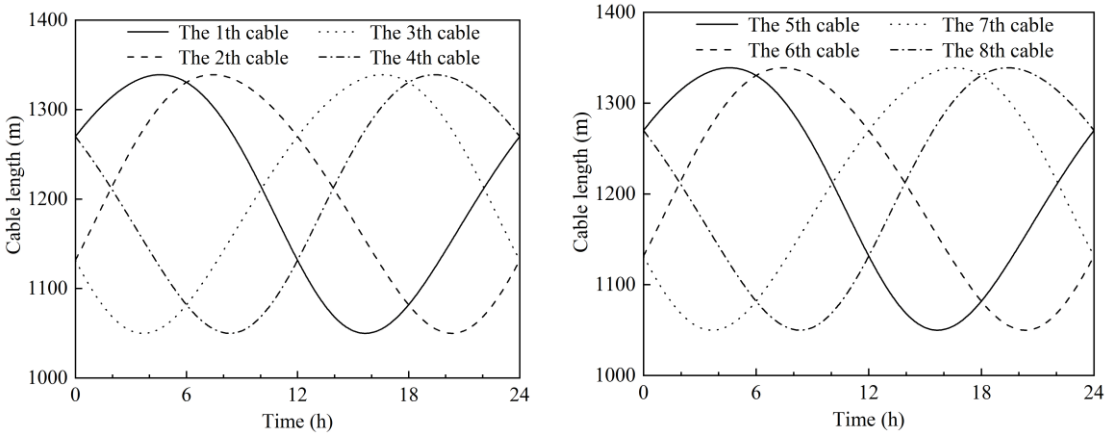

Figure 9. Cable length change curve. (**a**) The up rail; (**b**) The down rail.

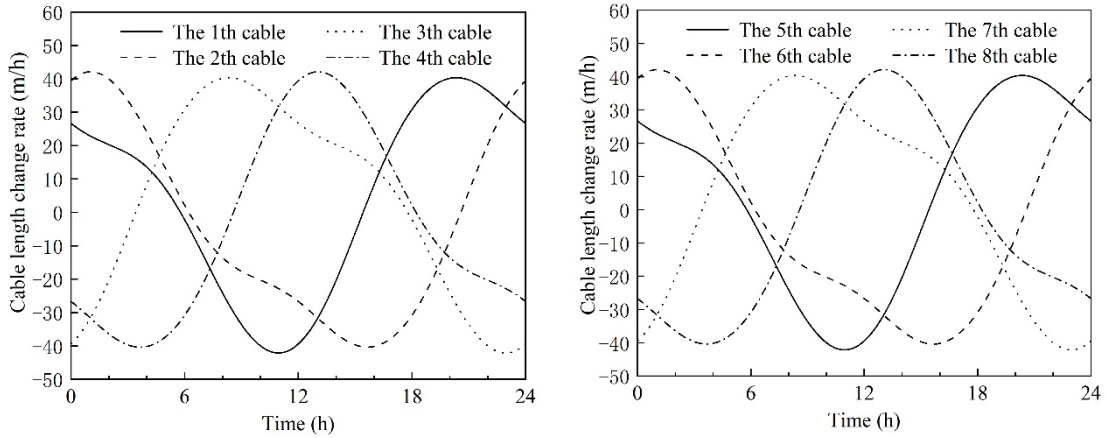

Figure 10. Cable length change rate curve. (**a**) The up rail; (**b**) The down rail.

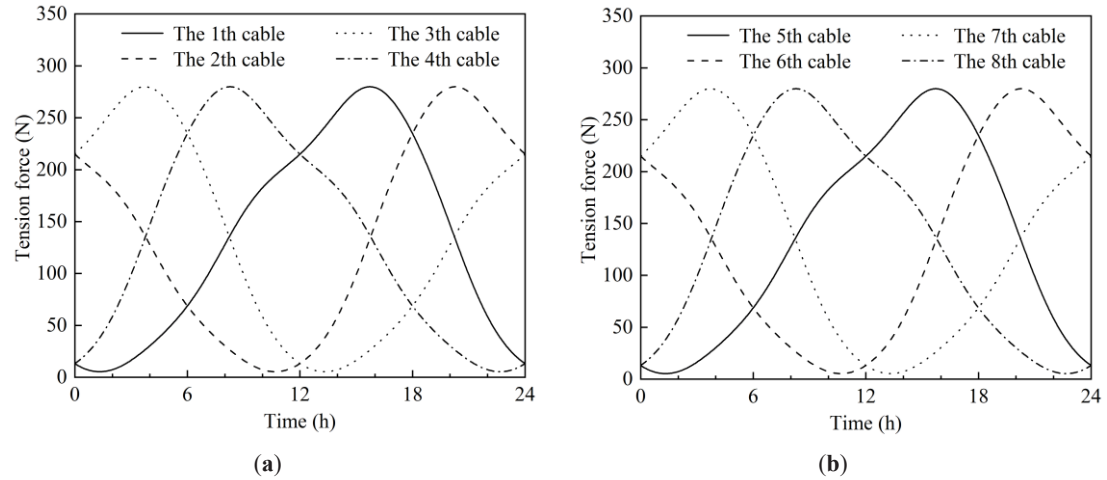

Figure 11. Tension force change curve. (**a**) The up rail; (**b**) The down rail.

6. Conclusions

In this paper, SSPS-OMEGA is taken as the research object, the motion planning of the subsystem is carried out, and the relative attitude change relationship between the condenser, the PV array and the transmitting antenna are studied. Based on the redundant cable solution method and design criteria, a scheme of eight parallel cable drive for transmitting antenna is designed. Through model construction and simulation analysis, the following conclusions are obtained:

(1) Considering the different orientation targets, due to the existence of ecliptic angle, the relative attitude between subsystems in OMEGA scheme presents a large angle periodic change, the maximum value of rolling angle and pitch angle change is equal to the magnitude of the ecliptic angle, and the maximum value of yaw angle change is only 2.36°.

(2) Due to the symmetry of OMEGA structure and relative motion between subsystems, the design of cable mechanism also adopts unilateral symmetry and upper and lower symmetry redundancy layout. According to the optimization objective of minimum variance of cable force and the design criteria of smooth continuity and lightweight, the optimal cable force variation trend is obtained, the maximum cable force is not more than 280 N, and the minimum tension is 5.4 N. The maximum change rate of cable length is 42 m/h, and the change is smooth, which is easy to adjust the relative attitude between the condenser and the transmitting antenna smoothly and continuously.

Author Contributions: X.J.: conceptualization, methodology, original draft preparation; G.F.: software, data curation; R.L.: supervision; J.S.: investigation; D.Z.: validation. All authors have read and agreed to the published version of the manuscript.

Funding: This work is supported by the Shandong Province Natural Science Foundation of China (NO. ZR2023QE100, and NO. ZR2022ME082), the Natural Science Basic Research Plan in Shaanxi Province of China (NO. 2024JC-YBQN-0489), the National Natural Science Foundation of China (No. 51976087), and the Youth Entrepreneurship Technology Support Program for Higher Education Institutions of Shandong Province (No. 2023KJ215).

Institutional Review Board Statement: Not applicable.

Informed Consent Statement: Not applicable.

Data Availability: Statement: Not applicable.

Conflicts of Interest: The authors declare no conflict of interest.

References

1. Glaser, P.E. Power from the sun: Its future. *Science* **1968**, *162*, 857–861.
2. Rouge, J.D. *Space-based Solar Power as an Opportunity for Strategic Security: Phase 0 Architecture Feasibility Study*; National Security Space Office: Arlington, VA, USA, 2007.
3. Seboldt W.; Klimke M.; Leipold M.; Hanowski N. European sail tower SPS concept. *Acta Astronaut.* **2001**, *48*, 785–792.
4. Sasaki S.; Tanaka K.; Higuchi K.; Okuizumi N.; Kawasaki S.; Shinohara N.; Senda K.; Ishimura K. A new concept of solar power satellite: Tethered-SPS. *Acta Astronaut.* **2007**, *60*, 153–165.
5. Carrington C.; Fikes J.; Gerry M.; Perkinson D.; Feingold H.; Olds J. The Abacus/Reflector and integrated symmetrical concentrator- Concepts for space solar power collection and transmission. In Proceedings of the 35th Intersociety Energy Conversion Engineering Conference and Exhibit, VegasLas, NV, USA, 24–28 July 2000.
6. Mankins J.; Kaya N.; Vasile M. *SPS-ALPHA: The First Practical Solar Power Satellite via Arbitrarily Large Phased Array*; Artemis Innovation Management Solutions LLC: Nipomo, CA, USA, 2012.
7. Hou X.; Wang L.; Zhang X.; Zhou L. Concept design on multi-rotary joints SPS. *J. Astronaut.* **2015**, *36*, 1332–1338.
8. Yang Y.; Zhang Y.; Duan B.; Wang D.; Li X. A novel design project for space solar power station (SSPS-OMEGA). *Acta Astronaut.* **2016**, *121*, 51–58.
9. Yang Y.; Zhang Y.; Fan G.; Li M.; Pei M. Construction strategy and performance analysis of large-scale spherical solar concentrator for the space solar power station. *Sol. Energy* **2020**, *207*, 133–143.
10. Ma X.; Li T.; Ma J.; Wang Z.; Shi C.; Zheng S.; Cui Q.; Li X.; Liu F.; Guo H.; et al. Recent Advances in Space-Deployable Structures in China. *Engineering* **2022**, *17*, 208–220.
11. Sun Z.; Yang D.; Duan B.; Kong L.; Zhang Y. Structural design, dynamic analysis, and verification test of a novel double-ring deployable truss for mesh antennas. *Mech. Mach. Theory* **2021**, 165, 104416.
12. Ishimura K.; Higuchi K. Coupling between structural deformation and attitude motion of large planar space structures suspended by multi-tethers. *Acta Astronaut.* **2007**, *60*, 691–710.
13. Fujii H.A.; Sugimoto Y.; Watanabe T.; Kusagaya T. Tethered actuator for vibration control of space structures. *Acta Astronaut.* **2015**, *117*, 55–63.

14. Landsberger, S. E. Design and construction of a cable-controlled parallel link manipulator. *Mass. Inst. Technol.* **1984**, *22,* 2317.
15. Tang X.; Chai X.; Tang L.; Shao Z. Accuracy synthesis of a multi-level hybrid positioning mechanism for the feed support system in FAST. *Robot. Comput. -Integr. Manuf.* **2014**, *30*, 565–575.
16. Qiu Y.; Duan B.; Wei Q.; Nan R.; Peng B. Optimal distribution of the cable tensions and structural vibration control of the cable-cabin flexible structure. *Struct. Eng. Mech.* **2002**, *14*, 39–56.
17. Zi B.; Duan B.; Du J.; Bao H. Dynamic modeling and active control of a cable-suspended Parallel robot. *Mechatronic* **2008**, *18*, 1–12.
18. Mikelsons, L.; Bruckmann, T.; Hiller, M.; Schramm, D. A real-time capable force calculation algorithm for redundant tendon-based parallel manipulators. In Proceedings of the 2008 IEEE International Conference on Robotics and Automation, Pasadena, CA, USA, 19–23 May 2008; IEEE: Piscataway, NJ, USA, 2008; pp. 3869–3974.
19. Borgstrom P.H.; Jordan B.L.; Sukhatme G.S.; Batalin M.A.; Kaiser W.J. Rapid computation of optimally safe tension distributions for parallel cable-driven robots. *IEEE Trans. Robot.* **2009**, *25*, 1271–1281.
20. Gosselin C.; Grenier M. On the determination of the force distribution in overconstrained cable-driven parallel mechanisms. *Meccanica* **2011**, *46*, 3–15.
21. Ji X.; Zhang Y.; Fan G.; Li M.; Li X. Attitude control of space solar power satellite with large range of relative motion among subsystems. *Aerosp. Sci. Technol.* **2020**, 100, 105781.
22. Ji X.; Duan B.; Zhang Y.; Fan G.; Li M.; Yang Y. Effect of operational condition of rotational subsystem on attitude control for space solar power station. *Chin. J. Aeronaut.* **2021**, *34*, 289–297.
23. Su Y.; Qiu Y.; Liu P. The continuity and real-time performance of the cable tension determining for a suspend cable-driven parallel camera robot. *Adv. Robot.* **2015**, *29*, 743–752.